

## PAPER

[View Article Online](#)  
[View Journal](#) | [View Issue](#)Cite this: *Dalton Trans.*, 2024, **53**,  
5658Access to long-lived room temperature  
phosphorescence through auration of  
2,1,3-benzothiadiazole†Mauricio Posada Urrutia,<sup>†a</sup> Nidhi Kaul,<sup>†b</sup> Tobias Kaper,<sup>a</sup> Dustin Hurrell,<sup>c</sup>  
Linus Chiang,<sup>†c</sup> Jordann A. L. Wells,<sup>b</sup> Andreas Orthaber,<sup>†b</sup>  
Leif Hammarström,<sup>†b</sup> Lukasz T. Pilarski<sup>†a</sup> and Christine Dyrager<sup>†a\*</sup>

A series of 2,1,3-benzothiadiazole–Au(I)–L complexes have been synthesised, structurally characterised and investigated for their photophysical properties. These are the first organometallic Au(I) complexes containing a C–Au bond on the highly electron-deficient benzothiadiazole unit. The complexes exhibit solution-phase phosphorescence at room temperature, assigned to the intrinsic triplet state of the benzothiadiazole unit that is efficiently populated through its attachment to gold. Comparison with routinely reported Au(I) complexes, which include intervening alkenyl linkers, suggests that previous assignments of their phosphorescence as  $^1\pi \rightarrow \pi^*(C\equiv CR)$  might be incomplete. Our observations affirm that, in addition to the heavy atom effect, breaking symmetry in the involved aryl motif may be of importance in controlling the luminescence properties.

Received 25th January 2024,  
Accepted 26th February 2024

DOI: 10.1039/d4dt00238e

[rsc.li/dalton](http://rsc.li/dalton)

## Introduction

Organometallic Au(I) complexes have emerged as an attractive class of luminescent emitters with prospects for various applications, including OLED materials and chemical sensing.<sup>1–5</sup> Their luminescent behaviour is usually ascribed to the heavy-atom effect of gold that induces large spin–orbit coupling (SOC), which results in efficient intersystem crossing (ISC) from the singlet to the triplet excited state.<sup>6–8</sup> However, the presence of an Au atom does not always dramatically increase the intersystem crossing rate ( $k_{ISC}$ );<sup>9</sup> many emissive organometallic Au(I) structures display very weak phosphorescence or solely exhibit prompt or delayed fluorescence.<sup>4,9</sup> The two-coordinate linear geometry of Au(I) complexes also enables close aurophilic contacts (2.7–3.5 Å) between gold centres (Au⋯Au), which may affect the nature of the emission.<sup>6</sup>

The most extensively investigated class of luminescent Au(I) complexes are acetylene-based derivatives (exemplified by

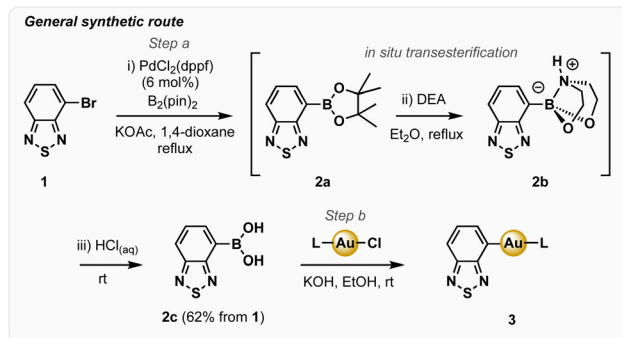
$R^1-C\equiv C-Au-R^2$ ).<sup>4,10,11</sup> Their emission has been attributed to the triplet excited state manifold of the alkynyl fragment.<sup>4,9</sup> The photophysics of aryl–Au(I)–L complexes (*i.e.*, with a direct aryl C–Au bond), however, has not been explored to the same extent or compared with the former in great detail. Also, the structural diversity of such emitters is relatively unexplored, especially species based on (hetero)aryl units beyond simple polycyclic aromatic hydrocarbons (PAHs).<sup>12–16</sup> An early report by Gray and co-workers described Au(I) pyrenyls exhibiting pyrene-based  $\pi \rightarrow \pi^*$  phosphorescence at 77 K.<sup>13</sup> More recently, Thompson and co-workers observed both inter-ligand charge transfer (ICT) and metal-to-ligand charge transfer (MLCT) emissions in aryl–Au(I)–NHC complexes at room temperature,<sup>17,18</sup> where changing the donor strength of the aryl group allowed for tuning between the two emissive states. Therefore, the organic unit in aryl–Au(I) complexes is not limited to acting merely as a relativistic spectator; the origin and characteristics of observed emissions can, in fact, largely depend on the aryl motifs, together with the position of auration. The development of aryl–Au(I) complexes that contain structurally and electronically diverse aromatic units is, therefore, a promising strategy for the discovery of new Au(I)-based luminophores.

As part of our ongoing research into harnessing the photophysical properties of BTD derivatives,<sup>19–22</sup> we sought to investigate BTD–Au(I) complexes as promising luminophores. Here, we report a series of emissive aryl–Au(I)–L complexes in which the gold centre is directly attached to the highly electron-

<sup>a</sup>Department of Chemistry-BMC, Uppsala University, Box 576 751 23, Uppsala, Sweden. E-mail: [christine.dyrager@kemi.uu.se](mailto:christine.dyrager@kemi.uu.se)<sup>b</sup>Department of Chemistry-Ångström, Uppsala University, Box 523, 751 20 Uppsala, Sweden<sup>c</sup>Department of Chemistry, University of the Fraser Valley, V2S7M8 Abbotsford, BC, Canada†Electronic supplementary information (ESI) available. CCDC 2026788 and 2125287–2125290. For ESI and crystallographic data in CIF or other electronic format see DOI: <https://doi.org/10.1039/d4dt00238e>

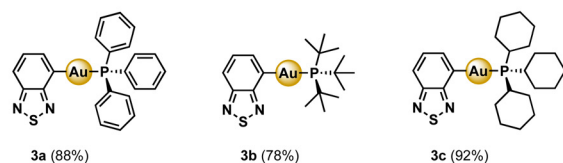
‡These authors contributed equally to this work.

deficient 2,1,3-benzothiadiazole (BTD) unit *via* a C–Au bond (Scheme 1). Hitherto, organometallic Au(I) luminophores based on fluorescent heteroaromatic chromophores (*e.g.*, coumarin, BODIPY, and BTD) have only been acetylides.<sup>4,9,11,23</sup> Among these are **BTD–C≡C–Au–PCy<sub>3</sub>** (reported by Che and co-workers in 2017, see Table 3), which exhibit prompt and delayed fluorescence.<sup>9</sup> We found that the absence of the acetylene linker precludes delayed fluorescence and instead grants access to long-lived (~100 μs) room temperature phosphorescence in solution. This feature arises due to the direct attachment of gold, which significantly enhances ISC to the triplet state and thereby amplifies the weak intrinsic phosphorescence of the parent BTD unit.<sup>24</sup> In this study, we gained important insight into the origins of this phosphorescence, as well as reconsidered the previous reported assignments for related acetylide-based luminophores.

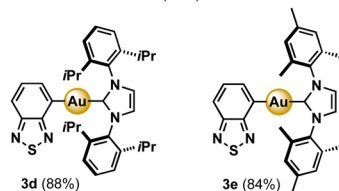


#### Scope in BTD–Au(I)–L complexes

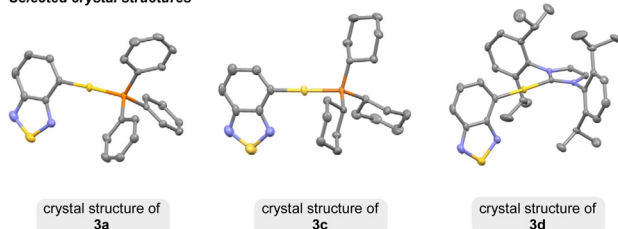
L = phosphine ligand



L = NHC ligand



#### Selected crystal structures



**Scheme 1** Top and middle: synthesis and scope of BTD–Au(I)–L complexes **3a–3e**. Conditions: (a) (i)  $B_2(\text{pin})_2$ , KOAc,  $\text{PdCl}_2(\text{dppf})$  (6 mol%), 1,4-dioxane, reflux, 90 min; (ii) diethanolamine (DEA),  $\text{Et}_2\text{O}$ , reflux, 30 min; (iii) 4 M  $\text{HCl}(\text{aq})$ , r.t., 5 min. 62% over 3 steps. (b)  $\text{L–Au–Cl}$ , KOH,  $\text{EtOH}$ , r.t., 24 h. Bottom: selected crystal structures of **3a**, **3c** and **3d**.

## Results and discussion

### Synthesis and characterisation

Novel BTD–Au(I) complexes **3a–e** were synthesised from **1** *via* Miyaura borylation (Scheme 1).<sup>25</sup> *In situ* deprotection of the corresponding pinacol boronate ester **2a**, *via* transesterification with diethanolamine (DEA) and acid hydrolysis of adduct **2b**, gave boronic acid **2c** in 62% overall yield.<sup>26,27</sup> The corresponding Au(I) complexes **3a–e** were generated in good to excellent yields (78–92%) *via* transmetalation between **2c** and L–Au(I)–Cl salts (L = phosphine, NHC) in  $\text{EtOH}$  at r.t.,<sup>13,28,29</sup> and were obtained as analytically pure, air-stable colourless solids that exhibit solid-state emission (ESI, Fig. S3†).

Complexes **3a–e** were characterised by  $^1\text{H}$ ,  $^{13}\text{C}$  and, where applicable  $^{31}\text{P}$  NMR spectroscopy, and high-resolution mass spectrometry (HRMS). X-ray diffraction (XRD) data for all complexes **3a–e** is given in the ESI† and selected crystal structures of **3a**, **3c** and **3d** are shown in Scheme 1 (bottom panel). Importantly, none of the crystal structures show close intermolecular Au...Au interactions; the shortest distances range between 5.6–8.6 Å, which is beyond the limit for aurophilic contacts.<sup>6</sup>

### Electrochemical analysis

The electrochemical properties of THF solutions of **3a–e** were investigated using cyclic voltammetry. All the complexes exhibited irreversible redox waves at *ca.* 1 V vs.  $\text{Fc}/\text{Fc}^+$ , and no redox waves in the cathodic region of the voltammogram within the electrochemical window of the experiments (Table 1; ESI, Fig. S12–16 and Tables S8–12†). While a few BTD–M compounds (M = Pd,<sup>30</sup> Zn,<sup>31</sup> Ag,<sup>32</sup> Sn<sup>33</sup>) have been reported previously, their electrochemical or photophysical properties have not. As such, there is a lack of directly comparable examples for the electrochemical studies presented in this work. Conversely, the electrochemical properties of the alkyne linked analogue **BTD–C≡C–Au–PCy<sub>3</sub>** in  $\text{CH}_2\text{Cl}_2$  have been reported, where a BTD-acetylide-based reduction wave was observed at  $-1.94$  V vs.  $\text{Fc}/\text{Fc}^+$ , without a redox wave in the anodic region.<sup>9</sup> The lack of cathodic waves for **3a–e** suggests their reduction occurs at more negative potentials, likely outside the measured electrochemical window, implying the LUMO of complexes **3a–e** is higher in energy than that of their alkynyl-bridged congeners. On the other hand, anodic waves were observed for **3a–e**, while none were observed for their alkyne-containing analogue in  $\text{CH}_2\text{Cl}_2$ . This suggests the HOMO of **3a–e** is higher in energy in compari-

**Table 1** Electrochemical data for compounds **3a–e**<sup>a</sup>

BTD–Au(I)–L complex	$E_1$ (V)	$E_2$ (V)
<b>3a</b>	0.95	1.05
<b>3b</b>	1.13	—
<b>3c</b>	1.11	—
<b>3d</b>	1.15	—
<b>3e</b>	0.93	1.09

<sup>a</sup> Values were determined in THF at 298 K, referenced to a ferrocene standard. Supporting electrolyte: 0.1 M  $[\text{nBu}_4\text{N}]\text{PF}_6$ , scan rate: 100 mV  $\text{s}^{-1}$ .



son to **BTD-C≡C-Au-PCy<sub>3</sub>**. The origins of these frontier molecular orbitals were further investigated by density functional theory (DFT) computations (*vide infra*).

### Steady-state and time resolved photophysics

The photophysical properties of compound **3a–e** were investigated in 2-Me-THF (Table 2 and Fig. 1). All complexes absorb in the blue region (below ~400 nm) with two characteristic absorption bands; one centred at ~300 nm with some fine structure and a broader band at ~350 nm (Fig. 1A). Extinction coefficients for the latter range from 2800–5500 M<sup>−1</sup> cm<sup>−1</sup>.

Comparing the absorption spectra of **3a–e** with the spectrum of unsubstituted BTD suggests that the lowest energy band is a direct consequence of the auration. This observation differs from the explanation invoked for the alkynyl-bridged analogue **BTD-C≡C-Au-PCy<sub>3</sub>**, where the lowest energy band was attributed to dipole-allowed intraligand transitions of the alkynyl motif, <sup>1</sup>π → π\*(C≡CR), with some charge transfer character.<sup>9</sup> Furthermore, ligation of gold in **BTD-C≡C-Au-PCy<sub>3</sub>** was suggested to result in a bathochromic shift of the <sup>1</sup>IL band. However, given that the bridging alkynyl is entirely absent in **3a–e**, its involvement can be ruled out.

**Table 2** Photophysical data for the BTD-Au(I)-L complexes **3a–e** in 2-Me-THF<sup>a</sup>

BTD-Au(I)-L complex	UV/Vis absorption $\lambda_{\text{max}}/\text{nm}$ ( $\epsilon/\text{M}^{-1} \text{cm}^{-1}$ )	Emission				
		$\lambda_{\text{em}}, \lambda_{\text{phos}}^b$ (nm)	$\lambda_{\text{phos}}$ at 77 K <sup>c</sup> (nm)	$\tau_{\text{PF}}^d$ (ns)	$\tau_{\text{phos}}^e$ (μs)	$\Phi_{\text{phos}}^f$
<b>3a</b>	306 (13 600), 313 (13 400), 346 (5500)	415, 621	622	2	96	0.03
<b>3b</b>	305 (11 900), 312 (12 000), 349 (4300)	416, 624	624	2	88	0.03
<b>3c</b>	305 (11 900), 312 (10 900), 349 (3900)	416, 625	624	2	104	0.04
<b>3d</b>	305 (9800), 312 (7200), 356 (3800)	416, 631	629	2	102	0.04
<b>3e</b>	305 (7300), 312 (7200), 356 (2800)	415, 630	629	2	100	0.06

<sup>a</sup> Data were obtained from steady-state measurements using degassed 2-Me-THF solutions of **3a–e** (15 μM) at 298 K unless otherwise specified. <sup>b</sup>  $\lambda_{\text{ex}} = 355$  nm. <sup>c</sup> Measurements at 77 K were performed in the presence of air. <sup>d</sup> Emission lifetimes of prompt fluorescence ( $\tau_{\text{PF}}$ ) were determined using time-correlated single photon counting (TCSPC) measurements, see ESI† for details. <sup>e</sup> Phosphorescence lifetimes ( $\tau_{\text{phos}}$ ) were determined using time resolved emission measurements. <sup>f</sup> Phosphorescence quantum ( $\Phi_{\text{phos}}$ ) yields were obtained using [Ru(bpy)<sub>3</sub>][PF<sub>6</sub>]<sub>2</sub> in aerated acetonitrile ( $\Phi_{\text{phos}} = 0.018$ )<sup>36</sup> as the standard.  $\Phi_{\text{phos}}$  values are rounded to the nearest centesimal.

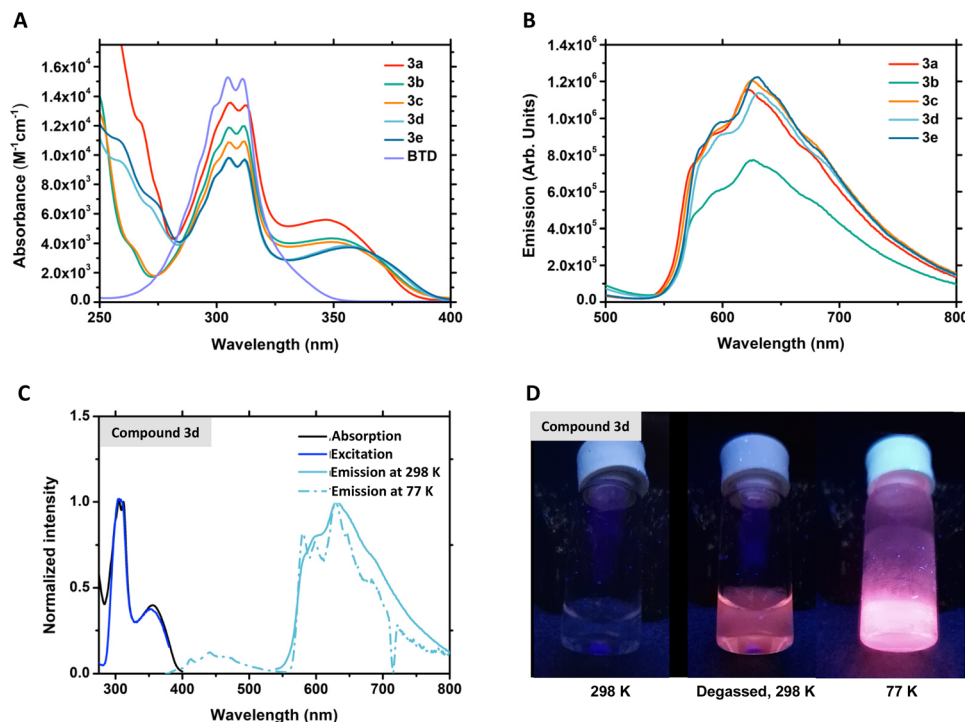


**Fig. 1** Photophysical data in 2-Me-THF. (A) UV-Vis absorption spectra for **3a–3e** at room temperature (conc. 15 μM). (B) Emission spectra for **3a–3e** (conc. 15 μM) recorded between 540–800 nm.  $\lambda_{\text{ex}} = 355$  nm (C) UV-Vis absorption spectrum, excitation spectrum (monitored at 620 nm) and emission spectrum (degassed compound,  $\lambda_{\text{ex}} = 355$  nm) for **3d** at room temperature plotted together with the emission spectrum of **3d** at 77 K (glassy matrix,  $\lambda_{\text{ex}} = 355$  nm) D) compound **3d** in 2-Me-THF. Left vial: at room temperature, 298 K, in the presence of air; middle vial: degassed (N<sub>2</sub> sparged) solution at 298 K; right vial: glassy matrix at 77 K in the presence of air.  $\lambda_{\text{ex}} = 365$  nm.



A better understanding into the origin of the lowest energy band for **3a–e** can be obtained by considering the detailed spectroscopic analysis of BTB's transitions (which has been reported in the literature).<sup>24,34,35</sup> Accordingly, the first two electronically allowed  $^1\pi\pi^*$  transitions at 306 nm and 328 nm have been assigned as  $^1A_1 \leftarrow ^1A_1$  and  $^1B_2 \leftarrow ^1A_1$ , respectively, with about a fifth of the latter's intensity being sourced in  $^1A_1 \leftarrow ^1A_1$  as well. The former band is strong and does not shift upon auration. The latter band is weak and hard to resolve in the solution spectra of the unsubstituted BTB. The dominant vibration, characterizing this weak intensity band, is a fully symmetric ( $a_1$ )  $C_4C_5C_9$  angle bend with a ring contraction (ESI, Fig. S2†). The  $B_2$  vibrations also contribute and indulge in Herzberg–Teller intensity stealing, however, presumably from the  $^1A_1 \leftarrow ^1A_1$  band.<sup>35</sup> Since the Au(i) centre is directly ligated in the C4-position of **3a–e**, it can be rationalised that this band becomes more allowed and is bathochromically shifted due to the auration. Moreover, changing the auxiliary ligand from phosphine to carbene (NHC) resulted in a small but discernible redshift of the lowest energy absorption band, which indicates some minimal charge transfer (CT), considering that NHCs are generally stronger  $\sigma$ -donors than phosphine ligands.

At room temperature, excitation at 355 nm into the lowest energy absorption band of **3a–e** results in bright orange-red phosphorescence, in both the solid phase and degassed solutions. The latter has emission maxima between 621 nm and 630 nm (Fig. 1B). Phosphorescent quantum yields ( $\Phi_{\text{phos}}$ ) range between 0.03 and 0.06, which are notable for mononuclear Au(i) complexes in solution at room temperature. Lifetimes close to a hundred microseconds (ESI, Fig. S5†) also support the triplet nature of the red emission (Stokes shift of ca. 12 500  $\text{cm}^{-1}$ ).

We note that some recently reported Au(i)–carbene complexes show no or very low phosphorescence at room temperature in solution ( $\Phi \leq 0.01$ ), and that the phosphorescence lifetimes of these reached at best 41  $\mu\text{s}$  under such conditions.<sup>18</sup> Further work from Thompson and co-workers shows emissive Au(i)–carbene complexes with lifetimes up to 3.3  $\mu\text{s}$  in solution, though the emission was not ascribed primarily to ligand centred phosphorescence.<sup>17</sup> The photoluminescence of these complexes originated from a variety of states including ICT and MLCT. The comparatively large phosphorescence quantum yield for the compounds presented here, as well as their long lifetime, is again reinforced. Previous reports have described phosphorescent BTB derivatives in the solid state,<sup>37,38</sup> at 77 K,<sup>24,37</sup> and in solution.<sup>37,39</sup> However, for the solution-based phosphors the quantum yields have peaked at only 0.7%.<sup>39</sup> The longest lifetime that has been previously observed for a BTB derivative at room temperature solution has also remained modest, at 5.4  $\mu\text{s}$ . To date and to the best of our knowledge, the phosphorescence quantum yield and phosphorescence lifetime described in this study remain the largest for BTB-based phosphors in solution at room temperature.

The vibrational spacings seen for **3a–e** are similar to those observed for the very weak phosphorescence of the parent BTB

(observed only when deuterated or in halogenated solvents at 77 K)<sup>24</sup> suggesting an orbital parentage with  $^3\pi \rightarrow \pi^*$  character from the BTB unit. Furthermore, the emission intensity of **3a–e** in solution is significantly higher at 77 K (glassy matrix) than at room temperature (*cf.* **3d**, Fig. 1D). Changing the auxiliary ligand, from phosphine to NHC, also results in a small but discernible redshift of the emission as well as the absorption;<sup>28</sup> some charge transfer (CT) is thus indicated. The excitation spectra monitored at 620 nm unambiguously traces the ground state absorption spectrum, including the lowest energy band, which is characteristic of the complexes (Fig. 1C and ESI, Fig. S4†).

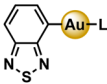
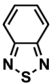
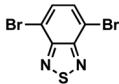
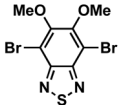
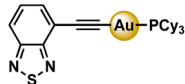
Complexes **3a–e** also exhibit prompt fluorescence ( $\lambda_{\text{max}} \sim 415$  nm), with lifetimes longer than unsubstituted BTB<sup>37</sup> ( $\tau \sim 2$  ns; ESI, Fig. S6†). It can therefore be inferred that auration alters the intrinsic photophysics. At higher laser excitation power (*s*), a low degree of photodegradation (<1% from the absorption data) was observed. This was evident by the appearance of strong emission signals at approximately 475 nm with lifetimes of a few tens of nanoseconds. Notably, these signals are identical to those reported for highly emissive Au nanoparticles/clusters<sup>40</sup> and should therefore not be mistaken for delayed fluorescence. The phosphorescence in our study is spectrally distinct from Au nanoparticle luminescence. Based on the prompt fluorescence lifetime of 2 ns ( $k_{\text{obs}} = 5 \times 10^8 \text{ s}^{-1}$ ) in the complexes, only the upper limit of the  $k_{\text{ISC}}$  can be estimated to  $10^8 \text{ s}^{-1}$  since the observed rate constant is the sum of all accessible decay pathways, which includes intersystem crossing. This would make it potentially an order of magnitude faster than the values reported for the alkynyl-bridged counterparts, which exclusively exhibit prompt and delayed fluorescence in solution.<sup>9</sup> It is worthwhile to note that the lifetimes and yields alone also do not permit for an evaluation of the intersystem crossing efficiency. Since  $\Phi_{\text{phos}} = \Phi_{\text{ISC}}[k_{\text{r}}/(k_{\text{r}} + k_{\text{nr}})]$  (where  $1/(k_{\text{r}} + k_{\text{nr}})$  is the observed phosphorescence lifetime),  $k_{\text{r}}$  and  $\Phi_{\text{ISC}}$  may not be disentangled.

Overall, the data suggest that a suitable photophysical descriptor for **3a–3e** is perturbation of the intrinsic emission behaviour of the heteroarene moiety by the Au(i) centre. Direct linkage to the gold, without the alkynyl linker in this case, can be thought to impact intersystem crossing rates favourably and enhance phosphorescence quantum yields in BTB. Support for such an analysis is found by comparing the aured BTB units presented in this study with Br-substituted BTB derivatives very recently reported in the literature,<sup>37</sup> as well as with the alkynyl bridged analogue reported by Che and co-workers.<sup>9</sup> The relevant structures, together with critical photophysical data at room temperature, is tabulated in Table 3. For **BTB–C≡C–Au–PCy<sub>3</sub>**, phosphorescence is exclusively observed at 77 K,<sup>9</sup> with very similar emission maxima and lifetime as for the complexes reported here (**3a–e**). On observing the trend in Table 3, it can be clearly seen that direct linkage of a heavy atom at the 4-position of BTB would make the weak  $^1B_2 \leftarrow ^1A_1$  transition more allowed due to broken symmetry, in conjunction with SOC. In fact, 4,7-dibromination is more effective for achieving BTB-based phosphorescence than introducing Au with an alkynyl linker (*cf.* **A** and **B** with **BTB–C≡C–Au–PCy<sub>3</sub>**).





**Table 3** Phosphorescent properties of various BTD derivatives at room temperature (r.t.); comparison of **3a–e** (this work) with previously reported BTD structures

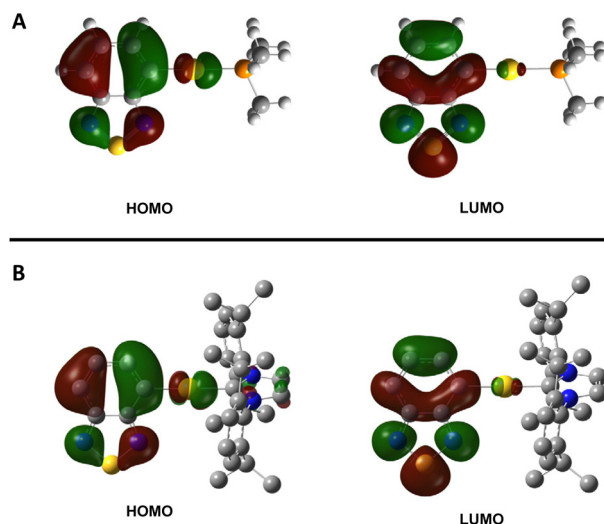
	<b>3a–e</b> (this work) <sup>a</sup>	<b>BTd</b> <sup>37</sup>	<b>A</b> <sup>37</sup>	<b>B</b> <sup>37</sup>	<b>BTd–C≡C–Au–PCy<sub>3</sub></b> <sup>9</sup>
Structure					
Phosphorescence ( $\Phi_{\text{phos}}$ , <sup>b</sup> $\lambda_{\text{max}}$ , <sup>c</sup> $\tau_{\text{phos}}$ <sup>d</sup> ) in:					
Solution, r.t.	0.04, 629 nm, 102 $\mu\text{s}$	Not observed	Not observed	<0.01, <sup>f</sup> 670 nm, <sup>f</sup> n.d. <sup>e</sup>	Not observed
Solid state, r.t.	n.d. <sup>e</sup>		<0.01, 685 nm, 37 $\mu\text{s}$	0.04, 648 nm, 585 $\mu\text{s}$	

<sup>a</sup> Values represent **3d** in 2-Me-THF. Table 2 contains photophysical data all complexes (**3a–e**). <sup>b</sup> Phosphorescence quantum yield,  $\Phi_{\text{phos}}$ . Values are rounded to the nearest centesimal or indicated as <0.01 if applicable. <sup>c</sup> Emission maxima,  $\lambda_{\text{max}}$  (nm). <sup>d</sup> Phosphorescence lifetimes,  $\tau_{\text{phos}}$  ( $\mu\text{s}$ ). <sup>e</sup> Not determined. <sup>f</sup> In THF.

For 4,7-dibromo-BTD (**A**), phosphorescence is only observed in the solid state and the yields remain well over an order of magnitude smaller than the solution phase yields of the complexes in the present work. Thus, the photophysical picture of accessing the triplet manifold of the heteroarene, *via* heavy atom substitution at the C4-position, is reinforced *via* direct auration of BTd.

### Computational studies

The absorption properties of **3a–e** were investigated computationally *via* DFT and TD-DFT calculations. The phenyl, *tert*-butyl and cyclohexyl moieties of **3a–c** were truncated to methyl groups, giving **BTd–Au–PMe<sub>3</sub>**, to expedite computations. For comparison, the same molecular truncation and computational parameters were applied to the previously reported acetylide analogue, giving **BTd–C≡C–Au–PMe<sub>3</sub>**, which resulted in frontier molecular orbitals (ESI, Fig. S8†) and vertical excitation energies (ESI, Tables S3 and 4†) that are near identical to those described in the literature.<sup>9</sup> Using this methodology, the frontier molecular orbitals of **BTd–Au–PMe<sub>3</sub>** (representing **3a–3c**) and **BTd–Au–NHCs** (**3d** and **3e**) were found to be similar to **BTd–C≡C–Au–PMe<sub>3</sub>**, comprising of the antibonding combinations of an Au d-orbital and a  $\pi$ -system of the BTd fragment (ESI, Fig. S9–11†). These orbitals are predominantly localised on the BTd fragment with minimal contribution from the  $\text{PMe}_3$  or the NHC ligands (Fig. 2). This is consistent with both the experimental observations of the auxiliary ligand showing a minimal contribution to the observed transitions, and the photophysics of the **BTd–Au(i)–L** complexes **3a–3e** being best described as a perturbation of that of the heteroarene moiety. Further, the TD-DFT calculated vertical excitation transitions of **BTd**, **BTd–Au–PMe<sub>3</sub>** and the **BTd–Au–NHCs** (**3d** and **3e**) originating from their respective HOMO and LUMO, reflects the observed trends, even if not the precise transition energies. The calculated orbitals for the HOMO and LUMO are consistent with symmetry labels A (symmetric with respect to the principal rotation axis) and B (anti-symmetric with respect to the principal rotation axis) for the  $C_{2v}$  point group of BTd. It can therefore represent the weaker symmetry-forbidden band at *ca.* 325 nm seen in experi-

**Fig. 2** HOMO and LUMO of (A) truncated **BTd–AuPMe<sub>3</sub>** and (B) **BTd–Au–NHC**.

ments. Meanwhile, the stronger band at *ca.* 300 nm is between the symmetric HOMO–1 and LUMO, *i.e.*,  $^1A_1 \leftarrow ^1A_1$ . In unsubstituted BTd, the computed oscillator strengths are consistent with such an analysis. Upon auration, the relative oscillator strengths of the two bands are reversed, reflecting the more allowed nature of the weaker band in **3a–e**, which is qualitatively captured at this level of theory. Finally, the predicted transitions of **BTd–Au–PMe<sub>3</sub>** are blue-shifted by  $4000\text{ cm}^{-1}$  in comparison to **BTd–C≡C–Au–PMe<sub>3</sub>**, consistent with their respective experimental absorption values (Table 2 and ESI, Tables S3–7†).<sup>9</sup>

The singlet ( $S_n$ ) and triplet ( $T_n$ ) excited state energies of **BTd–Au(i)–L** ( $L$  = truncated  $\text{PMe}_3$ , or NHCs: IPr and IMes) were investigated *via* TD-DFT calculations at their corresponding optimised singlet ground state ( $S_0$ ) geometries. For **BTd–Au–PMe<sub>3</sub>**, three triplet excited states ( $T_1$ – $T_3$ ) were found to be lower in energy than the lowest singlet excited state ( $S_1$ ), with the energy difference between the highest energy triplet ( $T_1$ ) and lowest energy singlet ( $S_1$ ) excited states ( $\Delta E_{\text{ST}}$ ) being  $12\,300\text{ cm}^{-1}$ , which falls in the proximity of the experimentally



observed difference between the fluorescence and phosphorescence spectral maxima (*ca.* 7500 cm<sup>-1</sup>). Similarly, both **3d** and **3e** exhibit five triplet excited states (T<sub>1</sub>–T<sub>5</sub>) lower in energy than the lowest singlet excited state (S<sub>1</sub>) and a small Δ*E*<sub>ST</sub> (**3d**: 12 000 cm<sup>-1</sup>; **3e**: 12 100 cm<sup>-1</sup>). Notably, while exclusively fluorescence or delayed fluorescence properties were reported for BTD–C≡C–Au–PCy<sub>3</sub>, **3a–c** exhibit phosphorescence. The observation of delayed fluorescence indicates that the triplet is also populated in the alkynyl-bridged complexes, but the radiative rate constant is not competitive. It can be hypothesised that direct coordination to Au results in a comparatively stronger SOC for **3a–3e**, resulting in a higher radiative rate constant, and the observed phosphorescent properties.

## Conclusions

A series of BTD–Au(I) complexes was synthesised, characterised (NMR, HRMS, CV and XRD) and investigated for their photo-physical behaviour. These are the first isolated coordination complexes containing a C–Au bond on the BTD unit and the first aryl–Au(I) complexes that comprise a highly electron-deficient heterocyclic unit. In solution the complexes display long-lived room temperature phosphorescence (*τ* ~ 100 μs) with appreciable quantum yields (*Φ*<sub>phos</sub> = 0.03–0.06). The origin of the phosphorescence was traced to the triplet manifold of BTD (<sup>3</sup>LC emission), which is efficiently populated specifically due to its direct auration. The strong phosphorescence compared to acetylene-linked Au(I) complexes suggest a larger radiative rate constant for the T<sub>1</sub>–S<sub>0</sub> transition, which can presumably be rationalised by a stronger SOC coupling with Au(I) directly linked on the BTD unit. In addition, the unsymmetrical substitution on BTD increases the oscillator strength of the lowest, symmetry-forbidden singlet–singlet transition of BTD and should also increase the rate constant for phosphorescence. This reveals the tantalising prospect that otherwise weak luminophores can form the basis of efficient organo–Au(I) phosphors with compact, simple, and robust motifs. We anticipate that this strategy may be generalisable for other weak luminophore/heavy atom combinations.

## Conflicts of interest

There are no conflicts to declare.

## Acknowledgements

This work was supported by the Swedish Research Council, Dnr: 2018-03524 (to CD) and a NSERC Discovery Grant, RGPIN-2018-06744 (to L. C.). Compute Canada is acknowledged for access to computational resources. This study made use of the NMR Uppsala infrastructure, which is funded by the Department of Chemistry – BMC and the Disciplinary Domain of Medicine and Pharmacy.

## References

- X. He and V. W.-W. Yam, *Coord. Chem. Rev.*, 2011, **255**, 2111–2123.
- E. E. Langdon-Jones and S. J. A. Pope, *Chem. Commun.*, 2014, **50**, 10343–10354.
- J. M. López-de-Luzuriaga, M. Monge and M. E. Olmos, *Dalton Trans.*, 2017, **46**, 2046–2067.
- M. Pujadas and L. Rodríguez, *Coord. Chem. Rev.*, 2020, **408**, 213179.
- X. Li, Y. Xie and Z. Li, *Chem. – Asian J.*, 2021, **16**, 2817–2829.
- H. Schmidbaur, *Gold Bull.*, 2000, **33**, 3–10.
- A. Vogler and H. Kunkely, *Coord. Chem. Rev.*, 2001, **219–221**, 489–507.
- H. Yersin, A. F. Rausch, R. Czerwieniec, T. Hofbeck and T. Fischer, *Coord. Chem. Rev.*, 2011, **255**, 2622–2652.
- K. T. Chan, G. S. M. Tong, W.-P. To, C. Yang, L. Du, D. L. Phillips and C.-M. Che, *Chem. Sci.*, 2017, **8**, 2352–2364.
- L. Gao, D. V. Partyka, J. B. Updegraff III, N. Deligonul and T. G. Gray, *Eur. J. Inorg. Chem.*, 2009, **2009**, 2711–2719.
- A. Möller, P. Bleckenwegner, U. Monkowius and F. Mohr, *J. Organomet. Chem.*, 2016, **813**, 1–6.
- M. Osawa, M. Hoshino and D. Hashizume, *Chem. Phys. Lett.*, 2007, **436**, 89–93.
- D. V. Partyka, A. J. Esswein, M. Zeller, A. D. Hunter and T. G. Gray, *Organometallics*, 2007, **26**, 3279–3282.
- W. Y. Heng, J. Hu and J. H. K. Yip, *Organometallics*, 2007, **26**, 6760–6768.
- L. Gao, M. A. Peay, D. V. Partyka, J. B. Updegraff III, T. S. Teets, A. J. Esswein, M. Zeller, A. D. Hunter and T. G. Gray, *Organometallics*, 2009, **28**, 5669–5681.
- R. A. Vogt, M. A. Peay, T. G. Gray and C. E. Crespo-Hernández, *J. Phys. Chem. Lett.*, 2010, **1**, 1205–1211.
- T.-y. Li, D. S. Muthiah Ravinson, R. Haiges, P. I. Djurovich and M. E. Thompson, *J. Am. Chem. Soc.*, 2020, **142**, 6158–6172.
- T.-y. Li, P. I. Djurovich and M. E. Thompson, *Inorg. Chim. Acta*, 2021, **517**, 120188.
- H. Appelqvist, K. Stranius, K. Borjesson, K. P. R. Nilsson and C. Dyrager, *Bioconjugate Chem.*, 2017, **28**, 1363–1370.
- K. Colas, S. Doloczki, A. Kesidou, L. Sainero-Alcolado, A. Rodriguez-Garcia, M. Arsenian-Henriksson and C. Dyrager, *ChemPhotoChem*, 2021, **5**, 632–643.
- K. Colas, K. O. Holmberg, L. Chiang, S. Doloczki, F. J. Swartling and C. Dyrager, *RSC Adv.*, 2021, **11**, 23960–23967.
- S. Doloczki, K. O. Holmberg, I. Fdez Galvan, F. J. Swartling and C. Dyrager, *RSC Adv.*, 2022, **12**, 14544–14550.
- A. Pinto, M. Echeverri, B. Gómez-Lor and L. Rodríguez, *Dalton Trans.*, 2022, **51**, 8340–8349.
- B. R. Henry and J. D. Morrison, *J. Mol. Spectrosc.*, 1975, **55**, 311–318.
- T. Ishiyama, M. Murata and N. Miyaura, *J. Org. Chem.*, 1995, **60**, 7508–7510.



- 26 J. Sun, M. T. Perfetti and W. L. Santos, *J. Org. Chem.*, 2011, **76**, 3571–3575.
- 27 P. A. Inglesby, L. R. Agnew, H. L. Carter and O. T. Ring, *Org. Process Res. Dev.*, 2020, **24**, 1683–1689.
- 28 F. J. L. Ingner, A.-C. Schmitt, A. Orthaber, P. J. Gates and L. T. Pilarski, *ChemSusChem*, 2020, **13**, 2032–2037.
- 29 For recent solvent-free approaches to the synthesis of organo-Au(i) complexes, see: (a) F. J. L. Ingner, Z. X. Giustra, S. Novosedlik, A. Orthaber, P. J. Gates, C. Dyrager and L. T. Pilarski, *Green Chem.*, 2020, **22**, 5648–5655; (b) G. Pisanò and C. S. J. Cazin, *ACS Sustainable Chem. Eng.*, 2021, **9**, 9625–9631.
- 30 K. Kubota, R. Takahashi and H. Ito, *Chem. Sci.*, 2019, **10**, 5837–5842.
- 31 H. Langhals, P. Knochel, A. Walter and S. Zimdars, *Synthesis*, 2012, 3465–3476.
- 32 T. S. Sukhikh, D. A. Bashirov, S. Shuvaev, V. Y. Komarov, N. V. Kuratieva, S. N. Konchenko and E. Benassi, *Polyhedron*, 2018, **141**, 77–86.
- 33 Y. Farré, M. Raissi, A. Fihey, Y. Pellegrin, E. Blart, D. Jacquemin and F. Odobel, *Dyes Pigm.*, 2018, **148**, 154–166.
- 34 J. M. Hollas and R. A. Wright, *Spectrochim. Acta, Part A*, 1969, **25**, 1211–1225.
- 35 R. D. Gordon and R. F. Yang, *J. Mol. Spectrosc.*, 1971, **39**, 295–320.
- 36 H. Ishida, S. Tobita, Y. Hasegawa, R. Katoh and K. Nozaki, *Coord. Chem. Rev.*, 2010, **254**, 2449–2458.
- 37 T. Ishi-i, R. Kichise, I. S. Park, T. Yasuda and T. Matsumoto, *J. Mater. Chem. C*, 2023, **11**, 3003–3009.
- 38 H. Shi, L. Zou, K. Huang, H. Wang, C. Sun, S. Wang, H. Ma, Y. He, J. Wang, H. Yu, W. Yao, Z. An, Q. Zhao and W. Huang, *ACS Appl. Mater. Interfaces*, 2019, **11**, 18103–18110.
- 39 G. D. Gutierrez, G. T. Sazama, T. Wu, M. A. Baldo and T. M. Swager, *J. Org. Chem.*, 2016, **81**, 4789–4796.
- 40 H. Kawasaki, K. Hamaguchi, I. Osaka and R. Arakawa, *Adv. Funct. Mater.*, 2011, **21**, 3508–3515.

